Validation of QGS and 4D-MSPECT for Quantification of Left Ventricular Volumes and Ejection Fraction from Gated ^{18}F-FDG PET: Comparison with Cardiac MRI

Wolfgang M. Schaefer, MD, PhD[1]; Claudia S.A. Lipke, MD[2]; Bernd Nowak, MD[1]; Hans-Juergen Kaiser, PhD[1]; Patrick Reinartz, MD[1]; Arno Buecker, MD[3]; Gabriele A. Krombach, MD[3]; Udalrich Buell, MD[1]; and Harald P. Kühl, MD[2]

[1]Department of Nuclear Medicine, University Hospital, University of Aachen, Aachen, Germany; [2]Medical Clinic I, University Hospital, University of Aachen, Aachen, Germany; and [3]Department of Radiology, University Hospital, University of Aachen, Aachen, Germany

The aim of this study was to validate Quantitative Gated SPECT (QGS) and 4D-MSPECT for assessing left ventricular end-diastolic and systolic volumes (EDV and ESV, respectively) and left ventricular ejection fraction (LVEF) from gated ^{18}F-FDG PET. **Methods:** Forty-four patients with severe coronary artery disease were examined with gated ^{18}F-FDG PET (8 gates per cardiac cycle). EDV, ESV, and LVEF were calculated from gated ^{18}F-FDG PET using QGS and 4D-MSPECT. Within 2 d (median), cardiovascular cine MRI (cMRI) (20 gates per cardiac cycle) was done as a reference. **Results:** QGS failed to accurately detect myocardial borders in 1 patient; 4D-MSPECT, in 2 patients. For the remaining 42 patients, correlation between the results of gated ^{18}F-FDG PET and cMRI was high for EDV ($R = 0.94$ for QGS and 0.94 for 4D-MSPECT), ESV ($R = 0.95$ for QGS and 0.95 for 4D-MSPECT), and LVEF ($R = 0.94$ for QGS and 0.90 for 4D-MSPECT). QGS significantly ($P < 0.0001$) underestimated LVEF, whereas no other parameter differed significantly between gated ^{18}F-FDG PET and cMRI for either algorithm. **Conclusion:** Despite small systematic differences that, among other aspects, limit interchangeability, agreement between gated ^{18}F-FDG PET and cMRI is good across a wide range of clinically relevant volumes and LVEF values assessed by QGS and 4D-MSPECT.

Key Words: gated ^{18}F-FDG PET; cardiovascular MRI; Quantitative Gated SPECT; 4D-MSPECT

J Nucl Med 2004; 45:74–79

Left ventricular cardiac volumes and left ventricular ejection fraction (LVEF) are reliable prognostic parameters for patients with coronary artery disease (CAD) (*1*,*2*). ^{18}F-FDG PET is widely used for identifying impaired but viable myocardium in patients with severe CAD (*3*).

Gated data acquisition in myocardial perfusion SPECT allows analysis of wall motion and calculation of end-diastolic and end-systolic volumes (EDV and ESV, respectively) and LVEF (*4*–*6*). The clinical relevance of wall motion analysis has been proven (*7*), and in a recent meta-analysis, volumetric analysis by gated SPECT was validated using cardiovascular cine MRI (cMRI) (*8*).

Given that ^{18}F-FDG PET has a higher spatial resolution than does perfusion SPECT and that dysfunctional but viable myocardium often shows preserved ^{18}F-FDG uptake but reduced perfusion tracer uptake, gated ^{18}F-FDG PET seems to be better suited than gated SPECT for calculating these parameters—especially in patients with severe CAD who are referred for myocardial viability diagnostics—even if the image quality of myocardial ^{18}F-FDG PET is more variable and dependent on physiologic parameters such as glucose and insulin levels than is the image quality of perfusion SPECT.

In a pilot study (*9*), we evaluated the use of Quantitative Gated SPECT (QGS; Cedars-Sinai Medical Center) for gated ^{18}F-FDG PET data after transformation into a SPECT-like format with a voxel size of 5.8 mm in side length. This new study was done on a larger patient cohort to validate the QGS and 4D-MSPECT (University of Michigan) algorithms for quantifying EDV, ESV, and LVEF using original (i.e., untransformed) gated ^{18}F-FDG PET data and to elucidate the characteristic differences between the 2 algorithms.

The method of reference chosen was cMRI because it allows an accurate (*10*), reproducible (*11*,*12*), and clinically relevant assessment of cardiac volumes and function with high temporal and spatial resolution. It is therefore best suited for a comparison with gated ^{18}F-FDG PET. Earlier studies evaluating QGS for gated ^{18}F-FDG PET used radionuclide angiography (*13*,*14*) as a reference method, and 2

Received May 9, 2003 (David's D.O.B.); revision accepted Oct. 3, 2003.
For correspondence or reprints contact: Wolfgang M. Schaefer, MD, PhD, Department of Nuclear Medicine, University Hospital, University of Aachen, Pauwelsstrasse 30, 52074 Aachen, Germany.
E-mail: wschaefe@nuk-gate.nukmed.rwth-aachen.de

studies with cine ventriculography (*15,16*) as a reference method used commercially unavailable algorithms to derive the global function from gated ^{18}F-FDG PET. However, none of these studies used as a reference a 3-dimensional dataset without any assumptions about left ventricular geometry.

MATERIALS AND METHODS

Patients

We examined 44 patients (37 male, 7 female; mean age, 65 ± 8 y; range, 48–81 y) who had severe CAD and were scheduled for routine ^{18}F-FDG PET to assess myocardial viability. Of these, 36 had a history of at least 1 previous myocardial infarction, 15 had 1-vessel disease, 9 had 2-vessel disease, and 20 had 3-vessel disease. Diabetes mellitus had previously been diagnosed in 13 patients. The mean fasting glucose level was 131 ± 61 mg/dL (range, 81–430 mg/dL). All patients gave informed consent for cMRI. The local ethics committee approved the study.

PET Methodology

PET scans were obtained on an ECAT EXACT 922/47 scanner (Siemens-CTI). All patients received 250 mg of acipimox 2 h before administration of ^{18}F-FDG. One hour before injection of ^{18}F-FDG, nondiabetic patients received an oral glucose load of 50 g to stimulate endogenous insulin secretion. Instead of receiving glucose, diabetics received insulin (3–30 IU) intravenously 5–10 min before administration of ^{18}F-FDG. Gated acquisition was done 60 min after intravenous administration of 283 ± 38 MBq of ^{18}F-FDG, dividing the cardiac cycle into 8 equal intervals. The acquisition time was 30 min for emission (2-dimensional mode) and 15 min for transmission (^{68}Ge/^{68}Ga rod sources). After attenuation and scatter correction of the gated ^{18}F-FDG PET sinograms, reconstruction using filtered backprojection in a 128 × 128 matrix was done for all gates (Hanning filter; cutoff frequency, 0.4 Nyquist). A zoom factor of 1.525 was applied to obtain transverse images with an isotropic voxel size of 3.38 mm per side. The isotropic datasets were transferred to a Siemens e.soft workstation (Siemens Gammasonics Inc.), where they were reoriented on the transverse planes, with reorientation parallel first to the septum and then to the inferior wall. The resulting reoriented datasets were stored for analysis.

Quantification Using QGS and 4D-MSPECT

The reoriented datasets were loaded into fully automated QGS (*4,5*), which first determined the maximal-count midmyocardial surface. Next, rays were subtended normally to it and count profiles were extracted for each ray. Endocardial and epicardial boundaries were then estimated using an asymmetric gaussian fit of the count profiles.

Unlike QGS, the semiautomated 4D-MSPECT software (*6*) processes data on the basis of a 2-dimensional gradient image from which the initial estimates of the ventricle are made. Thereafter, a series of 1- and 2-dimensional weighted splines are used to refine the endocardial and epicardial surface estimates. In 10 patients, 4D-MSPECT did not adequately detect the estimated basal plane, and the basal planes were therefore adjusted using the interactive quality assurance module.

QGS failed to accurately detect myocardial borders in 1 patient, and 4D-MSPECT, in 2; thus, the algorithms together provided the EDV, ESV, and LVEF values for 42 patients in common.

cMRI Methodology and Data Analysis

Within a median of 2 d, all patients underwent cMRI on a 1.5-T Gyroscan ACS-NT (Philips Medical Systems) using a balanced fast-field echo sequence also known as true fast imaging with steady-state precession (*12*). Integrated SENSE (SENSitivity Encoding) technology allowed superior image quality because of the shorter acquisition time and the higher contrast-to-noise ratio. Patients were imaged in end-expiration using a dedicated cardiac synergy coil and breath-hold technique, with repetition and echo times of 3.1 and 1.5 msec, respectively, a flip angle of 65°, and a matrix of 256 × 256 (field of view, 350–400 mm). Twenty phases were obtained per cardiac cycle. The 10- to 15-min scanning protocol included the vertical and horizontal long axes of the left ventricle, on which the planning of the short axis was then based. From base to apex, the whole left ventricle was acquired with slices of 8-mm thickness, resulting in full-volume datasets for all patients.

Left ventricular function was assessed by determining the EDV, ESV, and subsequent LVEF using the cardiac analysis software package provided by the manufacturer. The examiner did not know the results of the gated ^{18}F-FDG PET analysis. After the cardiac base and apex were determined, the first gate in each series was defined as the end-diastolic phase, and the image with the smallest ventricular volume was defined as the end-systolic phase. The endocardial borders of both heart phases were traced manually, with the trabeculation and the papillary muscles segmented as part of the myocardium. Both EDV and ESV were then automatically computed by summing the cross-sectional areas contained by the endocardial borders of all analyzed short-axis slices (*10,11*). The LVEF, expressed as a percentage, was calculated as the stroke volume divided by the EDV.

Statistical Analysis

Statistical analysis was done using SPSS 10 (SPSS Inc.) and Origin 6.1 G (OriginLab Corp.) software. The data are shown as mean ± SD. The mean values of EDV, ESV, and LVEF were tested for significance using a *t* test for paired samples while applying Bonferroni correction for multiple comparisons. A normal distribution was shown for all parameters (Kolmogorov–Smirnov test). The degree of agreement was tested according to the method of Bland and Altman (*17*); the Bland–Altman limits (mean of the differences ± 2 SDs of the differences) are shown in the figures. Pearson correlation coefficients were also calculated. $P < 0.05$ was accepted as significant.

RESULTS

Table 1 shows EDV, ESV, and LVEF from cMRI, QGS, and 4D-MSPECT for the 42 patients for whom both algorithms were successful.

The correlation between the EDV of gated ^{18}F-FDG PET and the EDV of cMRI was very high for QGS ($R = 0.94$, Fig. 1A) and 4D-MSPECT ($R = 0.94$, Fig. 1C). The slope of the regression line was 1.00 for QGS and 1.03 for 4D-MSPECT. The correlation between the ESV of gated ^{18}F-FDG PET and the ESV of cMRI was very high for QGS ($R = 0.95$, Fig. 2A) and 4D-MSPECT ($R = 0.95$, Fig. 2C). The slope of the regression line was 0.99 for both QGS and 4D-MSPECT. The correlation between the LVEF of gated ^{18}F-FDG PET and the LVEF of cMRI was high for QGS

TABLE 1
Values of EDV, ESV, and LVEF from cMRI and Gated ^{18}F-FDG PET

Value (n = 42)	EDV (mL)			ESV (mL)			LVEF (%)		
	cMRI	4D-MSPECT	QGS	cMRI	4D-MSPECT	QGS	cMRI	4D-MSPECT	QGS
Mean ± SD	176 ± 53	178 ± 58	177 ± 56	118 ± 50	121 ± 52	126 ± 52	34.9 ± 10.7	33.8 ± 8.7	30.6 ± 7.6
Range	87–328	85–344	87–345	42–247	52–281	59–271	12–59	18–53	16–47
P vs. cMRI		NS	NS		NS	NS		NS	<0.0001

NS = not statistically significant.

(R = 0.94, Fig. 3A) and 4D-MSPECT (R = 0.90, Fig. 3C). The slope of the regression line was 0.66 for QGS and 0.72 for 4D-MSPECT.

Bland–Altman analysis revealed no systematic error for estimation of EDV by QGS or 4D-MSPECT (Figs. 1B and 1D), with Bland–Altman limits of −39 to +39 mL for QGS and −43 to +39 mL for 4D-MSPECT. Bland–Altman analysis revealed no systematic error for estimation of ESV by QGS or 4D-MSPECT (Figs. 2B and 2D), with Bland–Altman limits of −38 to +24 mL for QGS and −35 to +30 mL for 4D-MSPECT. However, Bland–Altman analysis of LVEF by QGS (limits, −5% to +13%) revealed that LVEF is underestimated by QGS, in comparison with cMRI, with the underestimation showing a tendency to be greater in ventricles with a good LVEF (Fig. 3B). By contrast, with limits of −9% to +11%, Bland–Altman analysis revealed no systematic error or tendency toward error for estimation of LVEF by 4D-MSPECT (Fig. 3D).

The correlation between the results of 4D-MSPECT and QGS was very high for EDV (R = 0.99, Fig. 4A) and ESV (R = 0.99, Fig. 4C). For LVEF, the correlation was somewhat high (R = 0.90, Fig. 4E). The Bland–Altman limits were − 20 to +16 mL for EDV (Fig. 4B), −13 to +22 mL for ESV (Fig. 4D), and − 11% to +4% for LVEF (Fig. 4F).

DISCUSSION

Correlation and agreement analysis between gated ^{18}F-FDG PET and cMRI revealed an excellent correlation between both methods for EDV and ESV for either algorithm, with comparable Bland–Altman limits (Figs. 1 and 2). For LVEF, QGS correlated slightly better with cMRI but showed significant underestimation and a regression line slope of 0.66 (ideally 1), whereas 4D-MSPECT showed no significant underestimation but a slightly lower R value (R = 0.90 vs. R = 0.94) (Fig. 3) and a regression line slope of 0.72. The ranges of the Bland–Altman limits were comparable. In the pilot study (*9*), we proposed that the main reason for the underestimation of LVEF by QGS was the much lower temporal resolution of gated ^{18}F-FDG PET (8

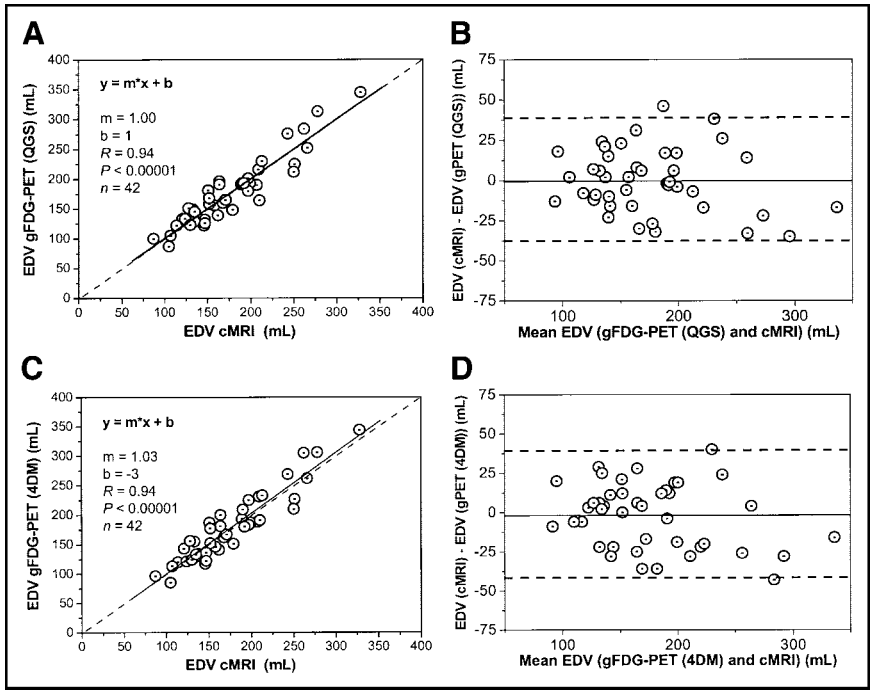

FIGURE 1. Correlation analysis of EDV estimated with QGS (A) and 4D-MSPECT (C) from gated ^{18}F-FDG PET and cMRI. Bland–Altman plots compare QGS versus cMRI (B) and 4D-MSPECT versus cMRI (D). 4DM = 4D-MSPECT; gFDG-PET and gPET = gated ^{18}F-FDG PET.

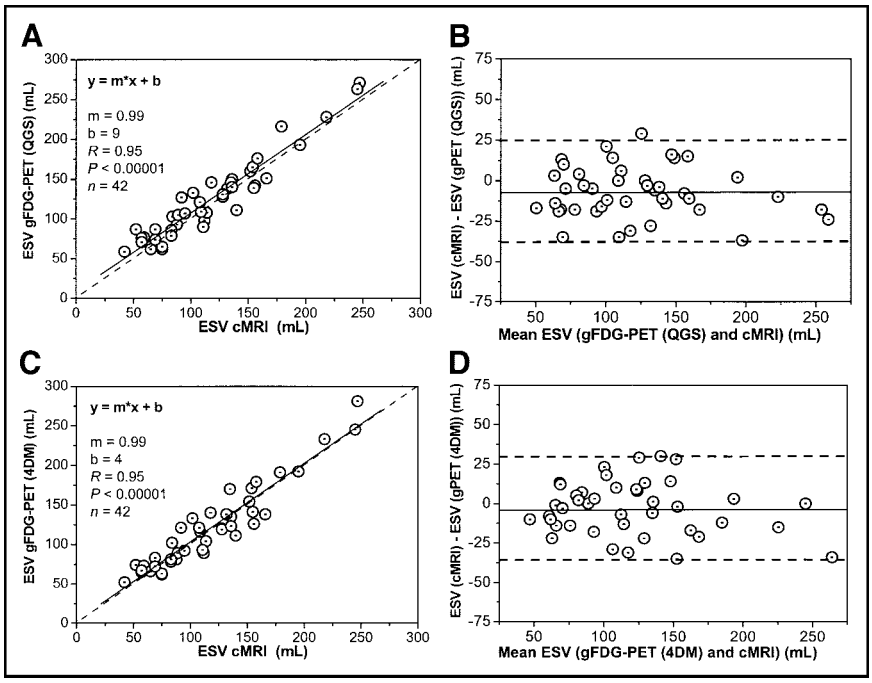

FIGURE 2. Correlation analysis of ESV estimated with QGS (A) and 4D-MSPECT (C) from gated ^{18}F-FDG PET and cMRI. Bland–Altman plots compare QGS versus cMRI (B) and 4D-MSPECT versus cMRI (D). 4DM = 4D-MSPECT; gFDG-PET and gPET = gated ^{18}F-FDG PET.

gates per cardiac cycle) than of cMRI (20 gates per cardiac cycle), but it remains unclear why this effect fell short of significance with 4D-MSPECT. The assumption that the reduced temporal resolution of gated ^{18}F-FDG PET causes LVEF underestimation agrees with the findings of Kumita et al. (*18*), who evaluated data from the same study using, first, 8 gates per cycle and then 16 gates per cycle, which yielded smaller EDV, larger ESV, and significantly smaller LVEF values in the 8-gates-per-cycle analysis. This phenomenon resulting in the reduced regression line slopes seems to be more obvious in ventricles with a good LVEF (Figs. 3A and 3C), since they are less hypocontractile, thereby increasing the relevance of differences in temporal resolution. Earlier studies using gated ^{18}F-FDG PET showed lower correlations for LVEF than did our study (R = 0.90 and 0.94) with the respective reference method (R = 0.86 (*13*), R = 0.83 (*14*), R = 0.84 (*15*), R = 0.75 (*16*)), but because none of these studies used a 3-dimensional reference method, volumes could not be calculated. The regression coefficients from the metaanalysis by Ioannidis et al.

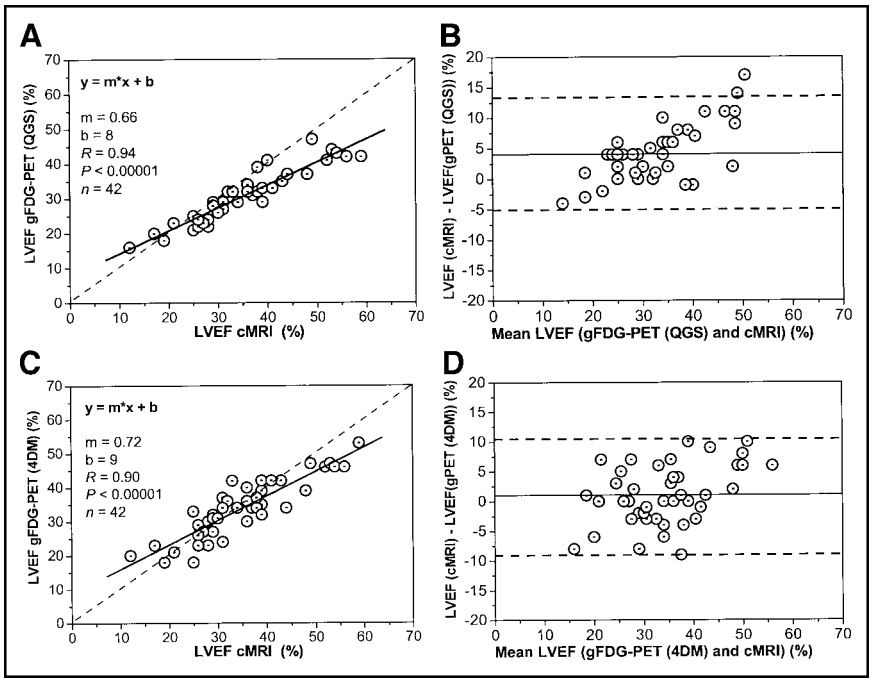

FIGURE 3. Correlation analysis of LVEF estimated with QGS (A) and 4D-MSPECT (C) from gated ^{18}F-FDG PET and cMRI. Bland–Altman plots compare QGS versus cMRI (B) and 4D-MSPECT versus cMRI (D). 4DM = 4D-MSPECT; gFDG-PET and gPET = gated ^{18}F-FDG PET.

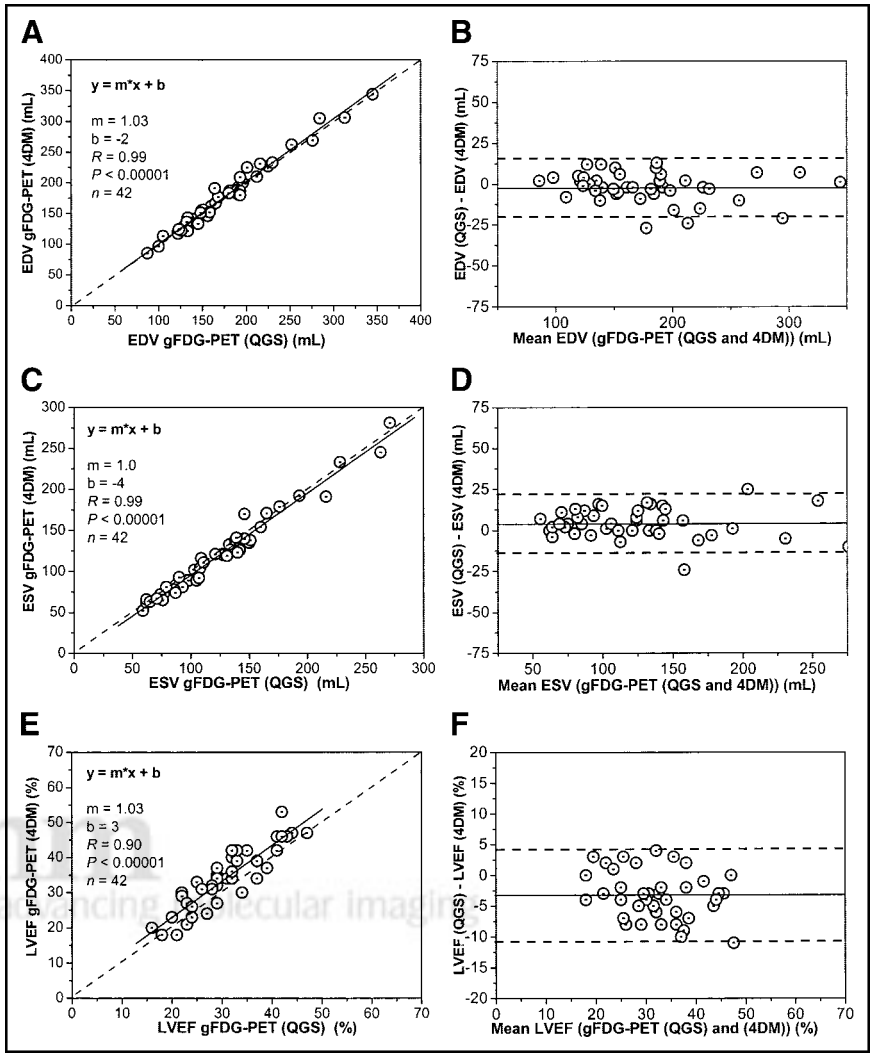

FIGURE 4. Correlation analysis of EDV (A), ESV (C), and LVEF (E) estimated with QGS and 4D-MSPECT from gated ^{18}F-FDG PET. Bland–Altman plots compare QGS versus 4D-MSPECT for EDV (B), ESV (D), and LVEF (F). 4DM = 4D-MSPECT; gFDG-PET = gated ^{18}F-FDG PET.

(*8*) were lower than ours, but even more important, their Bland–Altman limits were much wider than those in this study.

A study using gated ^{13}N-NH_3 PET (*19*) showed good results for LVEF, compared with the results from the excellent (and validated) gated ^{15}O-CO PET (*20*). However, the short half-life of ^{13}N (10 min) requires an on-site cyclotron, restricting the suitability of ^{13}N-NH_3 PET. Moreover, the fact that "hibernating myocardium" frequently shows perfusion deficits while glucose metabolism is preserved would also argue for gated ^{18}F-FDG PET instead of gated perfusion PET, where delineation may be complicated by perfusion deficits (*19*).

Direct comparison of QGS and 4D-MSPECT (Fig. 4) gave a better correlation and/or smaller Bland–Altman limits for all parameters than for both algorithms versus cMRI. This result was obviously due to the fact that both QGS and 4D-MSPECT evaluation used the same gated ^{18}F-FDG PET dataset. The correlation coefficients were nearly identical, as was evident from a direct comparison of QGS and 4D-MSPECT used with gated perfusion SPECT (*21*). However, all these comparisons may have underestimated the power of gated ^{18}F-FDG PET, since the ventricles we examined were more severely compromised (mean LVEF, 30%–35%) than those normally present in gated perfusion SPECT studies.

CONCLUSION

Despite small systematic differences, agreement between gated ^{18}F-FDG PET and cMRI is good across a wide range of EDV, ESV, and LVEF values calculated using QGS and 4D-MSPECT. Hence, with both algorithms, gated ^{18}F-FDG PET provides clinically relevant information on cardiac function and volumes. However, since, particularly, the LVEF values of these methods seem to diverge somewhat, the 2 methods should not be used interchangeably.

ACKNOWLEDGMENTS

Thanks are due to Ulrike Goeggel, Simone Dettki, and Monika Rohner for technical assistance and to Alejandro Rodón for general and language editing. This project was

funded by a grant from the IZKF BIOMAT (TV20/21, BMBF project 01 KS 9503/9) of Germany.

REFERENCES

1. Yamaguchi A, Ino T, Adachi H, et al. Left ventricular volume predicts postoperative course in patient with ischemic cardiomyopathy. *Ann Thorac Surg.* 1998;5:434–438.
2. White HD, Norris RM, Brown MA, Brandt PW, Whitlock M, Wild CJ. Left ventricular end-systolic volume as the major determinant of survival after recovery from myocardial infarction. *Circulation.* 1987;76:44–51.
3. vom Dahl J, Altehoefer C, Sheehan FH, et al. Recovery of regional left ventricular dysfunction after coronary revascularization: impact of myocardial viability assessed by nuclear imaging and vessel patency at follow-up angiography. *J Am Coll Cardiol.* 1996;28:948–958.
4. Germano G, Kiat H, Kavanagh PB, et al. Automatic quantification of ejection fraction from gated myocardial perfusion SPECT. *J Nucl Med.* 1995;36:2138–2147.
5. Iskandrian AE, Germano G, VanDecker W, et al. Validation of left ventricular volume measurements by gated SPECT ^{99m}Tc-labeled sestamibi imaging. *J Nucl Cardiol.* 1998;5:574–578.
6. Ficaro EP, Quaife RA, Kritzman JN, Corbett JR. Accuracy and reproducibility of 3D-MSPECT for estimating left ventricular ejection fraction in patients with severe perfusion abnormalities [abstract]. *Circulation.* 1999;100(suppl):I26.
7. DePuey EG, Rozanski A. Using gated technetium-99m-sestamibi SPECT to characterize fixed myocardial defects as infarct or artifact. *J Nucl Med.* 1995;36:952–955.
8. Ioannidis JP, Trikalinos TA, Danias PG. Electrocardiogram-gated single-photon emission computed tomography versus cardiac magnetic resonance imaging for the assessment of left ventricular volumes and ejection fraction: a meta-analysis. *J Am Coll Cardiol.* 2002;39:2059–2068.
9. Schaefer WM, Lipke C, Nowak B, et al. Validation of an evaluation routine for left ventricular volumes, ejection fraction and wall motion from gated cardiac FDG PET: a comparison with cardiac magnetic resonance imaging. *Eur J Nucl Med Mol Imaging.* 2003;30:545–553.
10. Dulce MC, Mostbeck GH, Friese KK, Caputo GR, Higgins CB. Quantification of the left ventricular volumes and function with cine MRI: comparison of geometric models with three-dimensional data. *Radiology.* 1993;188:371–376.
11. Sandstede J, Lipke C, Beer M, et al. Age- and gender-specific differences in left and right ventricular cardiac function and mass determined by cine magnetic resonance imaging. *Eur Radiol.* 2000;10:438–442.
12. Moon J, Lorenz C, Francis J, Smith G, Pennell D. Breath-hold FLASH and FISP cardiovascular MR imaging: left ventricular volume differences and reproducibility. *Radiology.* 2002;223:789–797.
13. Willemsen AT, Siebelink HJ, Blanksma PK, Paans AM. Automated ejection fraction determination from gated myocardial FDG-PET data. *J Nucl Cardiol.* 1999;6:577–582.
14. Saab G, Dekemp RA, Ukkonen H, Ruddy TD, Germano G, Beanlands RS. Gated fluorine 18 fluorodeoxyglucose positron emission tomography: determination of global and regional left ventricular function and myocardial tissue characterization. *J Nucl Cardiol.* 2003;10:297–303.
15. Hattori N, Bengel FM, Mehilli J, et al. Global and regional functional measurements with gated FDG PET in comparison with left ventriculography. *Eur J Nucl Med.* 2001;28:221–229.
16. Hor G, Kranert WT, Maul FD, et al. Gated metabolic positron emission tomography (GAPET) of the myocardium: ^{18}F-FDG-PET to optimize recognition of myocardial hibernation. *Nucl Med Commun.* 1998;19:535–545.
17. Bland JM, Altman DG. Statistical methods for assessing agreement between two methods of clinical measurement. *Lancet.* 1986;8476:307–310.
18. Kumita S, Cho K, Nakajo H, et al. Assessment of left ventricular diastolic function with electrocardiography-gated myocardial perfusion SPECT: comparison with multigated equilibrium radionuclide angiography. *J Nucl Cardiol.* 2001;8:568–574.
19. Okazawa H, Takahashi M, Hata T, Sugimoto K, Kishibe Y, Tsuji T. Quantitative evaluation of myocardial blood flow and ejection fraction with a single dose of $^{13}NH_3$ and gated PET. *J Nucl Med.* 2002;43:999–1005.
20. Rajappan K, Livieratos L, Camici PG, Pennell DJ. Measurement of ventricular volumes and function: a comparison of gated PET and cardiovascular magnetic resonance. *J Nucl Med.* 2002;43:806–810.
21. Nakajima K, Higuchi T, Taki J, Kawano M, Tonami N. Accuracy of ventricular volume and ejection fraction measured by gated myocardial SPECT: comparison of 4 software programs. *J Nucl Med.* 2001;42:1571–1578.